The Influence of the MJO on the Intraseasonal Variability of Northern Hemisphere Spring Snow Depth

BRADFORD S. BARRETT, GINA R. HENDERSON, AND JOSHUA S. WERLING

Oceanography Department, U.S. Naval Academy, Annapolis, Maryland

(Manuscript received 30 January 2015, in final form 10 June 2015)

ABSTRACT

Intraseasonal variability in springtime Northern Hemisphere daily snow depth change (ΔSD) by phase of the MJO was explored in this study. Principal findings of the relationship between ΔSD and the MJO included the following: 1) Statistically significant regions of lagged ΔSD anomalies for multiple phases of the MJO were found in March, April, and May in both North America and Eurasia. 2) In each month, lagged ΔSD anomalies were physically supported by corresponding lagged anomalies of 500-hPa height (Z500) and surface air temperature (SAT). Spearman rank correlation coefficients indicated a moderate to strong relationship between both Z500 and ΔSD and SAT and ΔSD in both Eurasia and North America for phases 5 and 7 in March. In April, a moderately strong relationship between Z500 and ΔSD was found over Eurasia for phase 5, but the relationship between SAT and ΔSD was weak. In May, correlations between ΔSD and both Z500 and SAT over a hemisphere-wide latitude band from 60° to 75°N were close to −0.5 and −0.4, respectively. Given the strength of these statistical relationships, the following physical pathway is proposed for intraseasonal variability of spring snow depth changes: poleward-propagating Rossby waves in response to tropical MJO convection interact with Northern Hemisphere background flow, leading to anomalous troughing and ridging. These anomalous circulation centers then impact daily snow depth change via precipitation processes and anomalies in surface air temperature.

1. Introduction

Tropical convective heating, including from the leading mode of atmospheric intraseasonal variability, the Madden–Julian oscillation (MJO; Madden and Julian 1971, 1972, 1994), forces a global atmospheric response in the form of poleward-extending wave trains (Hoskins and Karoly 1981; Sardeshmukh and Hoskins 1988; Jin and Hoskins 1995; Bladé and Hartmann 1995). These wave trains exert significant control over extratropical tropospheric circulation (Wallace and Gutzler 1981; Lau and Phillips 1986; Higgins and Mo 1997; Matthews et al. 2004; Jones et al. 2004; Weickmann and Berry 2009; Roundy et al. 2010; Riddle et al. 2013; Garfinkel et al. 2014). Because of this influence, high-latitude prediction at lead times longer than 4 or 5 days depends on the temporal evolution and geographical distribution of tropical convection of the MJO (Zhang 2005; Roundy 2012; Zhang 2013). Not surprisingly, Northern Hemisphere temperature (Lin and Brunet 2009; Zhou et al. 2012; Yao et al. 2011; Yoo et al. 2011, 2012; Rodney et al. 2013; Oliver 2015; Yoo et al. 2014; Johnson et al. 2014; Lin 2015) and precipitation (Bond and Vecchi 2003; Jeong et al. 2008; Lin et al. 2010; He et al. 2011; Becker et al. 2011; Jones and Carvalho 2014; Baxter et al. 2014) have both been found to vary significantly by MJO phase [in this article, MJO phase is defined using the methodology of Wheeler and Hendon (2004, hereafter WH04)]. However, Northern Hemisphere terrestrial snow depth has received relatively little attention, despite its established connection to anomalies in mid- to low-tropospheric circulation and surface air temperature (Déry and Brown 2007; Brown and Mote 2009; Mankin and Diffenbaugh 2015; Jackson et al. 2014; Rydzik and Desai 2014) and even snow accumulation over the Sierra Nevada of California (Guan et al. 2012). The objective of this study is to fill this gap by relating intraseasonal variability of spring snow depth to the MJO.

Snow depth, and particularly spring snow depth, was selected for study because it plays a critically important role in the cryosphere. The timing of spring snowmelt is particularly significant when considering such factors as low albedo of snow-free ground, snow acting as the

Corresponding author address: Bradford S. Barrett, 572C Holloway Road, Annapolis, MD 21402.
E-mail: bbarrett@usna.edu

DOI: 10.1175/JCLI-D-15-0092.1

frozen storage term in the water balance, and energy allocation involved with the warming and melting of snowpack (Derksen et al. 2014; Derksen and LeDrew 2000; Cohen and Rind 1991). The intraseasonal time scale was selected for study because as the MJO becomes more predictable (Vitart and Molteni 2010; Kang and Kim 2010; Neena et al. 2014; Zhu et al. 2014), understanding its influences on all aspects of the extratropics, including snow depth, allows for prediction beyond synoptic time scales (Goss and Feldstein 2015).

The MJO's modulation of the leading modes of high-latitude atmospheric circulation has been well documented. For example, the MJO has been found to affect the polarity of the Arctic Oscillation (Zhou and Miller 2005; L'Heureux and Higgins 2008), the North Atlantic Oscillation (Cassou 2008; Lin et al. 2009), and the Pacific–North America pattern (Mori and Watanabe 2008; Lin et al. 2009; Johnson and Feldstein 2010; Adames and Wallace 2014; Bao and Hartmann 2014). Via its modulation of large-scale circulation, the MJO's influence has already been found to extend to Arctic sea ice (Henderson et al. 2014). The primary pathway for MJO modulation of the extratropical circulation is via poleward-propagating Rossby waves. Seo and Son (2012) found that these Rossby waves were excited by horizontal divergence in the upper troposphere, and Matthews et al. (2004) found that as much as 35%–40% of the variance of upper-troposphere circulation can be explained by the MJO. The hypothesis tested in this study was that the MJO affects Northern Hemisphere snow depth via modulation of tropospheric circulation and surface air temperature. The remainder of this paper is organized as follows: datasets and methodology used are described in section 2, results are presented in section 3, and conclusions are presented in section 4.

2. Data and methods

This study spans a 33-yr period (1980–2013) and is focused on the intraseasonal variability of daily snow depth in the spring months of March to May (MAM). The decision to focus on spring snow depth change was based on several reasons. First, spring snowpack has been found to be critically important to seasonal hydrological variability (Hall et al. 2008; Koster et al. 2010; Zakharova et al. 2011; Mahanama et al. 2012) via impacts on soil moisture, streamflow, and feedbacks to air temperature. Second, spring snow impacts subsequent warm-season precipitation, both in terms of feedbacks over the northern Great Plains of North America, both positive (Quiring and Kluver 2009) and negative (Su et al. 2013), and through a negative feedback over monsoon areas (Gutzler and Preston 1997; Gutzler 2000; Zhu et al. 2005, 2007). Eurasian spring snow was found to have important feedbacks to Arctic sea ice (Matsumura et al. 2014), and the spring months (along with summer) showed less sensitivity to Arctic amplification (Francis and Vavrus 2015). Finally, spring months were selected because they exhibit some of the greatest interannual variability of snow depth (Ge and Gong 2008) and have potential for subseasonal variability (e.g., Derksen and Brown 2012; Wang et al. 2015). Given the role spring snow plays in a wide range of current and time-lagged atmospheric and hydrologic processes, it is critical to understand its variability on the intraseasonal time scale.

Three publicly available datasets are used to establish these connections between the MJO and snow depth. They are each described below.

a. *Atmospheric data*

To explore the state of the atmosphere under different lagged phases of the MJO, both at the surface and midtropospheric levels, geopotential height at 500 hPa (Z500) and surface air temperature (SAT) at 2 m were considered. Daily values of each field from the National Centers for Environmental Prediction (NCEP)–U.S. Department of Energy (DOE) AMIP-II reanalysis (Kanamitsu et al. 2002) product were examined. Daily composites of anomalous Z500 and SAT were created separately for each month, March through May, using the compositing methodology described below.

b. *MERRA snow depth*

Daily snow depth, in meters, was obtained from the Modern-Era Retrospective Analysis for Research and Applications (MERRA; Rienecker et al. 2011), NASA's current state-of-the-art reanalysis product, generated with version 5.2.0 of the Goddard Earth Observing System atmospheric model and data assimilation system. This reanalysis product is available globally on a $1.0° \times 0.67°$ latitude–longitude spatial scale for the years 1979–2014. Despite challenges associated with large-scale, gridded snow products, skill levels of MERRA snow depth and snow-water equivalent compared reasonably well against both in situ observations and other widely used large-scale snow products such as that of the Canadian Meteorological Center (Reichle et al. 2011). Although the MERRA-Land snow depth product (Reichle et al. 2011) appeared to have greater skill in representing snow depth, recent studies have documented spurious trend issues with the MERRA-Land product, including possible biases in precipitation from before 1999 (Trenberth et al. 2011). Daily change in snow depth (ΔSD) was calculated at each

Northern Hemisphere grid box during boreal spring months (MAM) using

$$\Delta SD = SD_{day_n} - SD_{day_{n-1}},$$

where SD_{day_n} is the daily snow depth for day n and $SD_{day_{n-1}}$ is the snow depth for the previous day. Mean monthly ΔSD (cm) for March, April, and May (Fig. 1) depicts snow depth decrease (green areas) and increase (purple areas) during each spring month. Not surprisingly for boreal spring, snow depth decrease dominates throughout the hemisphere during MAM, with the largest values of decrease migrating northward as the season progresses. Some areas of positive mean snow depth change were found in the farthest northern latitudes (poleward of 60°N) in both North America and Eurasia during March (Fig. 1a).

c. *MJO index and lagged composites*

The phase and amplitude of the MJO were defined using the daily real-time multivariate MJO (RMM) index (WH04). This index comprises the two leading principal components (PCs) of a multivariate empirical orthogonal function analysis, based on the input of daily outgoing longwave radiation and 850- and 200-hPa zonal wind fields. These two leading PCs are then used to classify the phase of MJO in eight different RMM phase spaces, corresponding roughly to the geographical location and intensity of enhanced convection on a particular day (WH04). The resulting index describes an MJO cycle that generally progresses eastward, from phase 1 to 8 and back to phase 1 again. Only days during which the RMM index had amplitude greater than 1 (amplitude is defined as the square root of $RMM1^2$ + $RMM2^2$; WH04), and therefore classified as "active," were considered for analysis. Such active days were used to filter both the atmospheric reanalysis data and the MERRA ΔSD data by phase of MJO, similar to the compositing methodology of other recent studies (e.g., Zhou et al. 2012; Virts et al. 2013; Zhang 2013; Barrett and Gensini 2013; Henderson et al. 2014).

Gridded composite anomalies of ΔSD, Z500, and SAT were calculated for each month and MJO phase at 7-day lags using the following process. First, for each MJO phase, mean Z500 and SAT at day_{n+7}, which was 7 days after an active MJO day_n, were calculated at each grid point. Mean ΔSD, 7 days after an active MJO day_n, was calculated as the snow depth on day_{n+7} minus the snow depth on day_{n+6}. In both cases, mean values included all days that meet the active MJO threshold, but no other tests (e.g., eastward propagation or consecutive-day active) were applied. Second, the 31-day long-term (1980–2013) mean values of Z500, SAT, and ΔSD

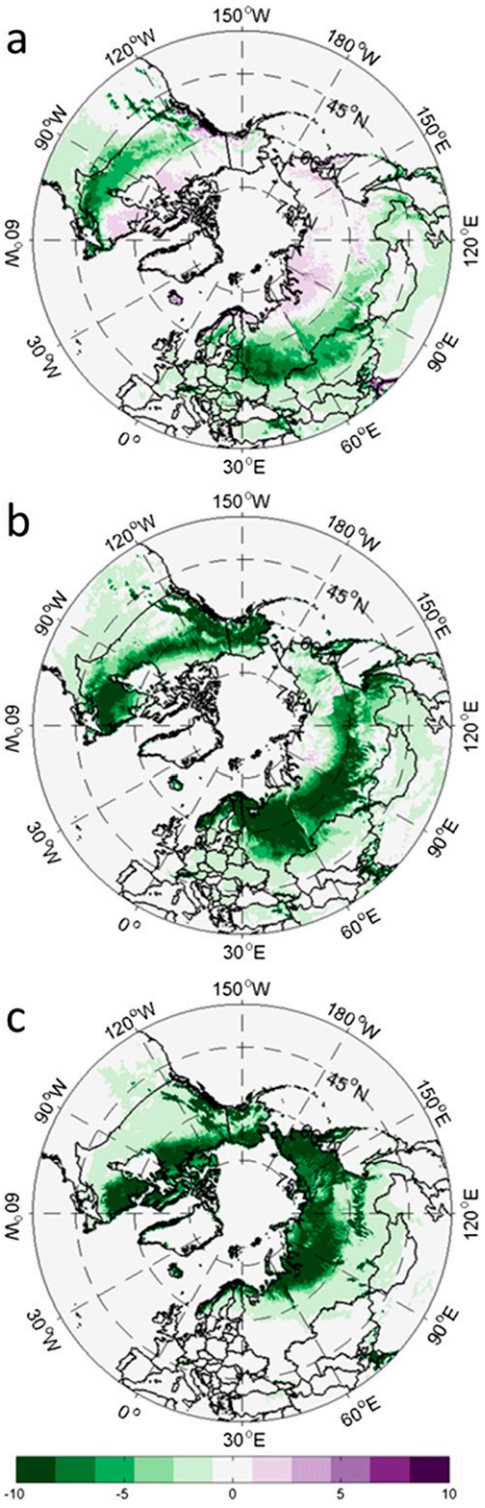

FIG. 1. Daily snow depth change expressed as a monthly average (cm day^{-1}) over 1980–2013 for (a) March, (b) April, and (c) May.

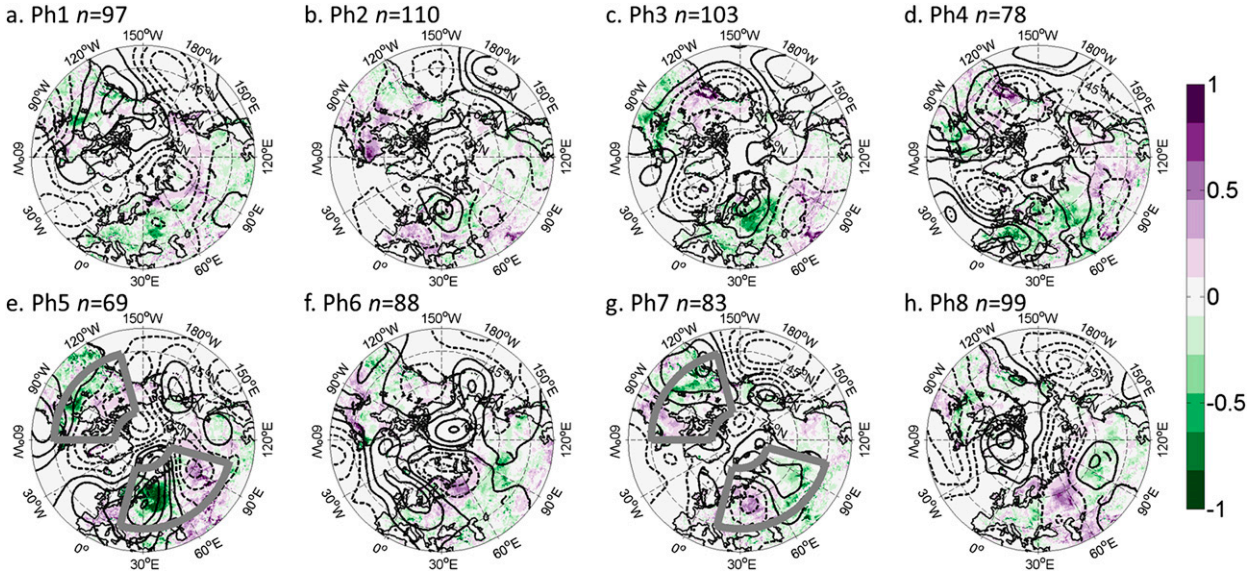

FIG. 2. March daily anomalies of snow depth change (shaded; cm day^{-1}) and 500-hPa height (black contours every 20 m; positive solid and negative dashed) at 7-day lags for active MJO phases (a) 1 to (h) 8. Gray bounded regions in (e),(g) indicate the Eurasian sector (45°–75°N, 15°–105°E) and the North American sector (45°–75°N, 135°–60°W). Data are from 1980 to 2013. All values of daily change in snow depth are statistically significant at the 95% level. Number of days in each phase is indicated by *n*.

centered on day$_{n+7}$ were subtracted to calculate lagged Z500, SAT, and ΔSD anomalies for that phase. Third, daily anomalies of Z500, SAT, and ΔSD were averaged for each month to calculate monthly anomalies for each MJO phase. Finally, ΔSD anomalies were tested for statistical significance using the Student's *t* test, and only those occurrences significant at the 95% confidence level were considered for analysis. Anomalies of ΔSD were examined at a 7-day lag following L'Heureux and Higgins (2008), Cassou (2008), Lin and Brunet (2009), and Flatau and Kim (2013), who found that the Northern Hemisphere extratropical response lagged tropical MJO convection by approximately 7 days.

3. Results

Each month was examined for intraseasonal variability of ΔSD, Z500, and SAT, and results for each spring month are presented below. Several patterns common to all months were seen. For example, ΔSD anomalies often exhibited wavy tendencies, whereby regions of positive ΔSD anomalies were located adjacent to regions of negative ΔSD anomalies. Additionally, ΔSD anomalies were often arranged in patterns of approximately synoptic scale (~1000 km) in size. Wavy synoptic-scale patterns were also seen in Z500 and SAT anomalies, and ΔSD, Z500, and SAT anomaly centers were often collocated and displayed moderate to strong correlations with each other. As such, the following physical pathway is proposed to explain possible intraseasonal variability in snow depth: anomalous tropical convection associated with the MJO drives Rossby wave propagation into the middle and high latitudes, and these anomalous troughs and ridges affect changes in surface snow depth either directly—via increased precipitation (as is found with anomalous troughing), decreased precipitation (as is found with anomalous ridging), or warmer surface air temperatures (as is found with ridging)—or indirectly, via colder surface air temperatures (as is found for troughing). Specific details for each month, including the phases where this pathway is most well developed, are presented below.

a. March

Anomalies of daily change in snow depth (ΔSD, cm day^{-1}) were examined at 7-day lags following active MJO days. In March, composite ΔSD anomalies for all eight phases exhibited statistically significant (at the 95% confidence level using a Student's *t* test) regions of both positive and negative ΔSD (Fig. 2). Furthermore, all eight phases featured regions of physically coherent variability, which in this study was defined as ΔSD anomalies that were found to be spatially uniform, of the same sign, and of approximately synoptic scale (~1000 km). For example, 7 days after active MJO phase 1 occurrences, negative ΔSD anomalies (as much as −1 cm day^{-1}) were located over most of Europe (Fig. 2a). As another example, 7 days after active MJO phase 2 occurrences, positive

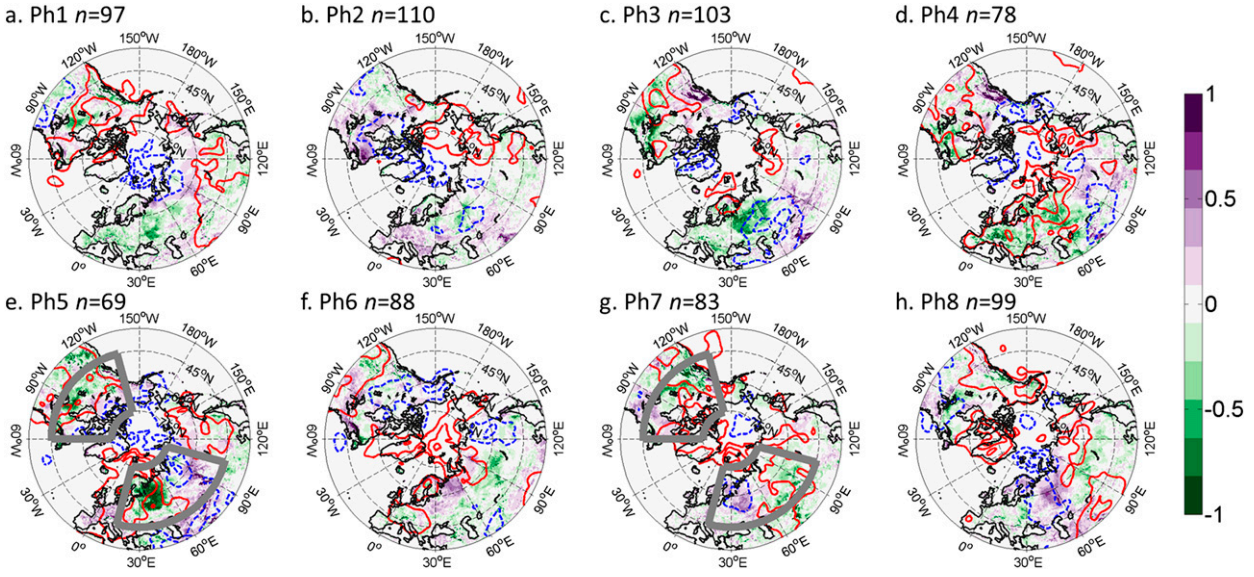

FIG. 3. (a)–(h) As in Fig. 2, but for March 1980–2013 surface air temperature anomalies (every 1 K; blue dashed contours indicate negative anomalies and red dashed contours indicate positive anomalies). Gray bounded regions in (e),(g) indicate the Eurasian sector (45°–75°N, 15°–105°E) and the North American sector (45°–75°N, 135°–60°W).

ΔSD anomalies (up to 1 cm day^{-1}) were located over eastern Canada (Fig. 2b). These types of synoptic-scale regions of spatially coherent ΔSD variability were found for all eight MJO phases. In addition to regions of spatially coherent variability, ΔSD anomalies were often found to exhibit dipole- and tripolelike patterns, whereby adjacent synoptic-scale areas of ΔSD anomalies were of opposite signs. One of the best examples of this pattern was seen in Eurasia: 7 days after active phase 5 occurrences, positive ΔSD anomalies (up to 1 cm day^{-1}) were found over western Europe, negative ΔSD anomalies (as much as −1 cm day^{-1}) were located over eastern Europe and western Russia, and negative ΔSD anomalies (up to −0.5 cm day^{-1}) were located over north-central Russia (Fig. 2e). Another example of dipole-structured ΔSD anomalies was found over North America, 7 days after active phase 7 (Fig. 2g), with a coherent region of negative ΔSD anomalies over western North America transitioning to a coherent region of positive ΔSD anomalies over eastern North America.

The atmospheric response at 500 hPa was also wavy, and synoptic-scale waviness was found at 7-day lags for all MJO phases (Fig. 2). Height anomalies at 500 hPa ranged from −80 to +80 m, and two phases with some of the largest anomalous Z500 were phases 5 and 7. For both of those phases, a defined wave train in height anomalies was found over much of the Northern Hemisphere. Ridging over eastern Europe and troughing over central Asia were noted for phase 5 (Fig. 2e), and an anomalous ridge–trough pattern over North America and a trough–ridge pattern over eastern Europe and western Asia were noted 7 days after active phase 7 days (Fig. 2g). In both phases, Z500 anomalies were mostly of the opposite sign of ΔSD anomalies. Surface air temperature anomalies in March typically ranged from −2 to +2 K, and anomalies of this magnitude were found for all phases (Fig. 3). In many phases, positive SAT anomalies (warmer temperatures) were collocated with negative ΔSD anomalies (indicative of more snow ablation, less accumulation, or anomalous snowpack metamorphosis), and negative SAT anomalies (colder temperatures) were collocated with positive ΔSD anomalies (indicative of either more snow accumulation or less ablation than normal). For phase 5, above-normal SAT anomalies were found over eastern Europe and most of Canada, while below-normal SAT anomalies were found over central Asia (Fig. 3e). For phase 7, above-normal temperatures were found over eastern Canada and central Asia, while below-normal temperatures were found over eastern Europe (Fig. 3g).

To quantify the relationship between ΔSD and Z500 and ΔSD and SAT seen particularly in phases 5 and 7, two subregions were selected for further analysis—one over eastern Europe and western Asia from 15° to 115°E and 45° to 75°N and another over northern North America from 140° to 60°W and 45° to 75°N (see gray sections in Figs. 2e,g). Spearman rank correlation coefficients between 7-day lagged ΔSD and Z500, and also lagged ΔSD and SAT, were calculated for each of these regions. Larger-magnitude correlations would indicate

TABLE 1. Spearman rank correlations between 500-hPa height and daily snow depth change as well as surface temperature and daily snow depth change for March 1980–2013. The Eurasian sector includes 45°–75°N, 15°–105°E, while the North American sector includes 45°–75°N, 135°–60°W. Bold values indicate the phase with the largest correlation coefficient.

March	Phase 1	Phase 2	Phase 3	Phase 4	Phase 5	Phase 6	Phase 7	Phase 8
Eurasia Z500	−0.21	−0.20	−0.37	−0.09	**−0.62**	−0.31	−0.56	−0.53
Eurasia SAT	0.01	0.27	0.22	−0.21	−0.37	0.32	**−0.55**	−0.43
North America Z500	−0.03	−0.01	−0.49	−0.28	−0.51	0.20	**−0.55**	−0.01
North America SAT	0.09	−0.05	−0.03	−0.15	**−0.45**	0.21	0.12	0.08

better physical agreement between the daily snow depth change and the surface air temperature or midtropospheric circulation anomalies. Rank correlations were also calculated over these two regions for the other six phases. Over the Eurasian region, correlation coefficients between ΔSD and Z500 were −0.62 in phase 5 and −0.56 in phase 7 (Table 1), suggesting a moderate to strong relationship between midtropospheric circulation anomalies and snow depth anomalies for those two phases over Eurasia. Correlation coefficients between ΔSD and SAT were −0.37 in phase 5 and −0.55 in phase 7, again suggesting a moderate relationship between snow depth changes and surface air temperature for those two phases. Over North America, correlations between ΔSD and Z500 7 days after active phases 5 and 7 were −0.49 and −0.54, respectively, and correlations between ΔSD and SAT were −0.45 and 0.12 for phases 5 and 7, respectively. These correlations indicate that for phase 5, circulation and temperature anomalies over North America were related to ΔSD anomalies, but that for phase 7, only circulation anomalies were related to ΔSD anomalies. All of the negative correlation coefficients for phases 5 and 7 were statistically significantly different from zero at the 99% confidence level. When calculated for all of North America (35°–75°N, 180°–15°W) and Eurasia (35°–75°N, 15°W–180°), correlation coefficients were smaller (closer to zero) for both SAT and Z500 (not shown).

These relationships agree with basic synoptic theory. Negative Z500 (troughing) and negative SAT (cold air) anomalies would be typically collocated with areas of positive ΔSD anomalies, and positive Z500 (ridging) and positive SAT (warm air) anomalies would be typically collocated with areas of negative ΔSD anomalies. More importantly, given that one of the primary extratropical atmospheric responses to the MJO is anomalous waviness in mid- and upper-tropospheric circulation (Hendon and Salby 1994; Kiladis et al. 2005; Barlow 2012; Monteiro et al. 2014; Adames and Wallace 2014), these moderate to strong correlations suggest the pathway for MJO to project onto daily snow depth change summarized at the outset of this section: poleward-propagating Rossby waves in response to tropical MJO convection interact with background flow, leading to anomalous troughing and ridging, which then directly impact snow depth via precipitation processes. Anomalous troughing and ridging also indirectly impact snow depth via anomalies in surface temperature, with colder temperatures associated with anomalous troughing and warmer temperatures associated with anomalous ridging. Over both Eurasia and North America, this modulation mechanism was not found to be uniform for all eight MJO phases, as correlations between ΔSD and Z500 and ΔSD and SAT were weak for most of the other phases. Given the moderate to strong Spearman correlation coefficients indicating a statistically significant relationship between ΔSD, Z500, and SAT anomalies, it is important to further explain the physical mechanisms by which the MJO could affect spring-season snow depth. Along the ephemeral snow zone, one physical interpretation of a negative correlation is that when surface air temperatures were above normal, physical processes such as above-normal snow melting, sublimating, or snowpack metamorphosis (including compaction) were favored. Another possible mechanism for such negative correlations is that when surface air temperatures were below normal, below-normal snow melting, sublimation, and compaction were favored, and furthermore, if precipitation was present, below-normal temperatures supported snow accumulation. All of these physical processes support negative correlations between SAT anomalies and ΔSD. At 500 hPa, negative correlations could have two possible physical mechanisms. First, positive Z500 anomalies would be associated with anomalous ridging and synoptic-scale processes that favor large-scale descent and reduced precipitation. Along the ephemeral snow zone, less-than-normal snow accumulation and greater-than-normal snow ablation (depending on the mean state of ΔSD as shown in Fig. 1) would both be favored from positive Z500 anomalies. Second, negative Z500 anomalies would be associated with anomalous troughing and processes that favor large-scale ascent and enhanced precipitation. Along the ephemeral snow zone, greater-than-normal snow accumulation and less-than-normal snow ablation would both be favored from negative Z500 anomalies. Each of these

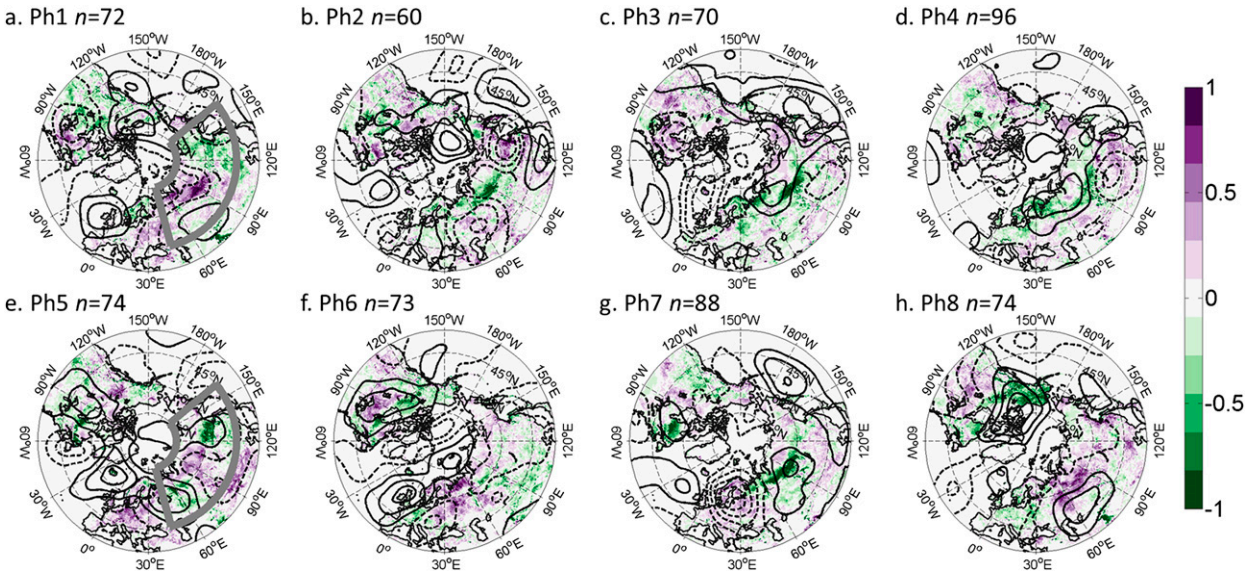

FIG. 4. (a)–(h) As in Fig. 2, but for April 1980–2013 snow depth change (shaded) and 500-hPa height (black contoured) anomalies. Eurasian sector indicated in (a),(e) by the gray bounded region (45°–75°N, 45°–160°E).

processes results from a negative correlation between ΔSD and Z500.

b. April

Similar to March, the most important result for April was that statistically significant (at the 95% confidence level) and physically coherent regions of ΔSD were found at 7-day lags for multiple MJO phases (Fig. 4). East–west-oriented dipole patterns in variability were particularly noted 7 days after active phase 1, 2, 4, 5, and 7 occurrences over different sections of Eurasia. The strongest positive ΔSD anomalies, up to $+1\,\mathrm{cm\,day^{-1}}$, were found 7 days after active phases 1, 5, and 8 (Figs. 4a,e,h), and the strongest negative ΔSD anomalies, up to $-1\,\mathrm{cm\,day^{-1}}$, were found 7 days after active phases 1, 2, 3, and 5. For phase 1, a dipole pattern was noted across Eurasia, with positive ΔSD anomalies near 90°E shifting to negative ΔSD anomalies near 120°E (Fig. 4a). For phase 5, a tripole pattern was noted extending from eastern Europe through to eastern Asia (Fig. 4e). Similar to March, the atmospheric response to MJO convection was in the form of wavy Z500 anomalies (Fig. 4). However, Z500 anomaly values were generally not as extreme, with anomaly centers of −30 to +30 m common for most phases (compared to −80 to +80 m for March). Despite this difference, the most significant Z500 anomaly centers still tended to be collocated with ΔSD anomalies of the opposite sign. For example, for phase 1, positive ΔSD anomalies were collocated with negative Z500 anomalies over north-central Eurasia (Fig. 4a), and for phase 5, a wave train of positive–negative–positive height anomalies extending across Eurasia was generally collocated with a similar tripole pattern in ΔSD (Fig. 4e). Surface air temperature anomalies in April were also similar to those in March, with −2 to +2 K anomalies found for multiple phases (Fig. 5). The strongest SAT anomaly centers tended to be collocated with ΔSD anomalies of the opposite sign. For example, positive SAT anomalies in eastern Asia for phase 1 were collocated with negative ΔSD anomalies (although over central Asia, positive ΔSD anomalies were located near positive SAT anomalies; Fig. 5a). For phase 5, negative SAT anomalies over western Asia and positive SAT anomalies over eastern Asia were collocated with positive and negative ΔSD anomalies, respectively (Fig. 5e). To quantify statistically the relationship between Z500 and ΔSD and SAT and ΔSD anomalies, Spearman rank correlation coefficients between Z500 and ΔSD and SAT and ΔSD were calculated over a Eurasian sector for each MJO phase. The sector was qualitatively identified from 45° to 160°E and 45° to 75°N, roughly corresponding to the dipole patterns in ΔSD anomalies seen for MJO phases 1 and 5 (Figs. 4a,e). The strongest correlation (−0.50) between Z500 and ΔSD was found for phase 5, with a slightly lower correlation (−0.42) found for phase 1 (Table 2). These correlations, statistically significantly different from zero at the 99% confidence level, corroborate the qualitative agreement seen in both phases 5 and 1, whereby positive snow depth change anomalies (purple shading) were generally collocated with negative Z500 anomalies (dashed contours), and negative snow depth change anomalies (green color) were generally

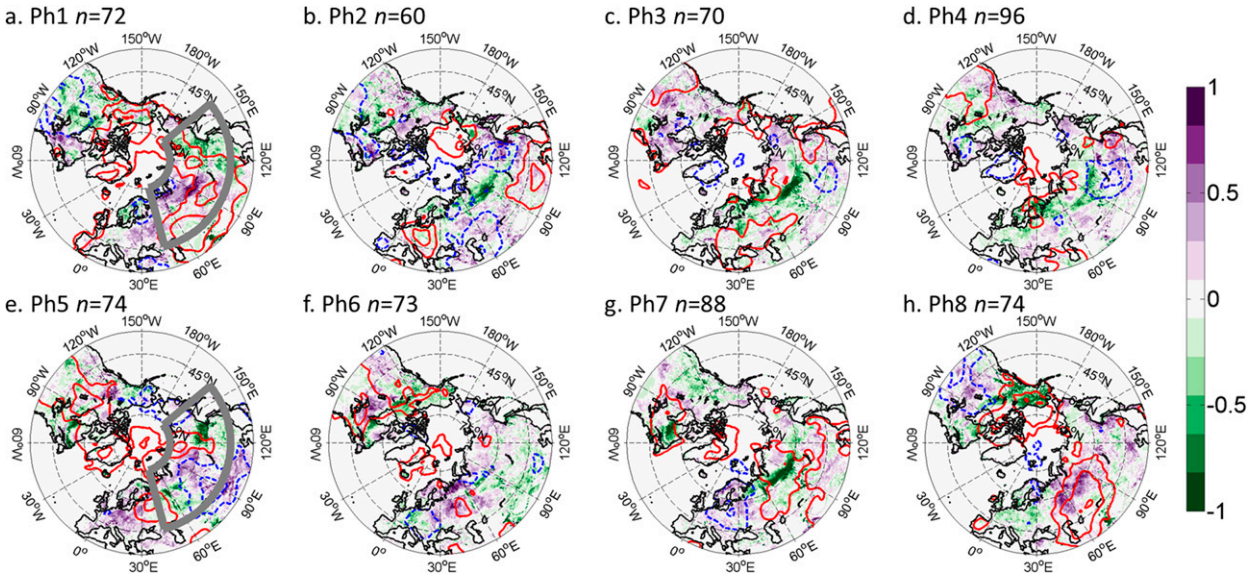

FIG. 5. (a)–(h) As in Fig. 3, but for April 1980–2013 snow depth change (shaded) and surface air temperature (blue and red contoured) anomalies. (a),(e) Eurasian sector indicated by the gray bounded region (45°–75°N, 45°–160°E).

collocated with positive Z500 anomalies (solid contours; Figs. 4a,e). Substantially smaller correlations were found between SAT and ΔSD in April: Spearman rank coefficients of −0.20 and −0.24 were found for phases 5 and 1, respectively (Table 2). While statistically significant, these correlations indicate only weak agreement between surface air temperature and snow depth changes in the Eurasian sector and highlight that the main source of intraseasonal variability of ΔSD in April was intraseasonal variability in midtropospheric circulation. Finally, when calculated for all of North America (35°–75°N, 180°–15°W) and Eurasia (35°–75°N, 15°W–180°), correlation coefficients were even smaller (closer to zero) for both SAT and Z500 (not shown).

Correlations in April between Z500 and ΔSD as well as SAT and ΔSD were less than in March (in March, the largest correlations exceeded −0.6 for Z500 and −0.5 for SAT). One possible explanation for this decline could be seasonal changes in snow extent from March to April. Throughout the hemisphere, snow extent declines significantly from March to April, from a monthly mean of approximately $4.037 \times 10^7\,km^2$ in March to $3.043 \times 10^7\,km^2$ in April, a decrease of 24.6% (Robinson et al. 1993). This decline in snow extent reduces the snow cover area and subsequently snow depth available to potentially experience modulation by the MJO. Given that these declines continue for May, it was not surprising to thus find even smaller areas of spatially coherent ΔSD anomalies by phase of MJO in that month.

c. May

The most notable result from May was that ΔSD anomalies were smaller in magnitude and spatial coverage than in both March and April. The largest-magnitude ΔSD anomalies were mostly confined to the high latitudes, poleward of 60°N (Fig. 6). For example, for the majority of MJO phases, dipole-shaped patterns and synoptic-scale coherent regions of ΔSD anomalies were generally seen only poleward of 60°N. Over northern Siberia, 7 days after active phase 1 occurrences, a positive–negative–positive–negative quadrupole in ΔSD anomalies was seen along 65°N extended from 45°E to 180° (Fig. 6a). Additionally, 7 days after active phase 3 occurrences, a region of coherent negative ΔSD anomalies aligned between 70° and 150°E and 45° and 75°N (Fig. 6c). The wavy pattern of Z500 anomalies resembled both March and April, with synoptic-scale waves seen for all phases. The magnitude of Z500 anomalies resembled April, regularly exceeding ±40 m. However, despite the

TABLE 2. As in Table 1, but for April 1980–2013. The Eurasian sector includes 45°–75°N, 45°–160°E.

April	Phase 1	Phase 2	Phase 3	Phase 4	Phase 5	Phase 6	Phase 7	Phase 8
Eurasia Z500	−0.42	−0.29	−0.17	−0.31	**−0.50**	0.07	−0.17	0.10
Eurasia SAT	**−0.24**	−0.03	0.02	0.15	−0.20	0.18	0.00	0.27

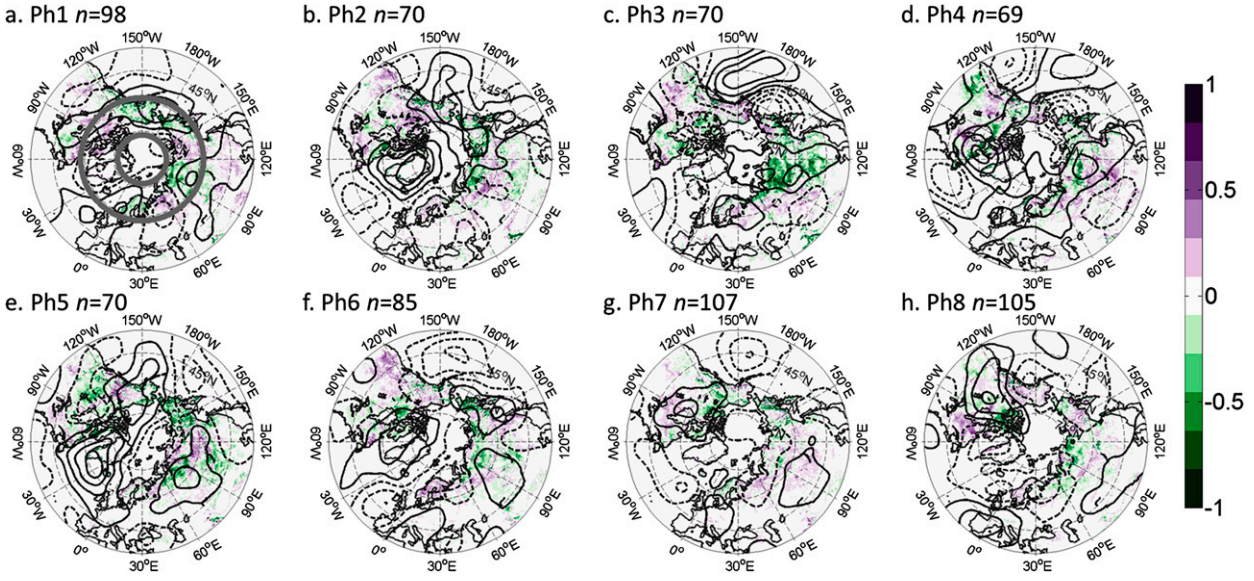

FIG. 6. (a)–(h) As in Fig. 2, but for May 1980–2013 snow depth change (shaded) and 500-hPa height (black contoured) anomalies. North American sector indicated in (a) by the gray bounded region includes all longitudes from 60° to 75°N.

similarities of May ΔSD and Z500 with March and April, very few regions of SAT anomalies below −1 or above +1 K exist (Fig. 7). Furthermore, perhaps only in one phase (phase 8; Fig. 7h) was there a region of spatially coherent SAT anomalies whose size approached synoptic scale.

To quantify the relationships between ΔSD and Z500 and SAT, Spearman rank correlation coefficients were calculated along a zonal band extending from 60° to 75°N. This zonal band was selected to try to capture variability within the ephemeral snow zone, which for May shifts to the north. The largest correlation coefficients were found for active phase 1 day, where coefficients of near −0.5 and −0.4 suggested a moderately strong physical relationship between ΔSD and Z500 and ΔSD and SAT, respectively (Table 3). Other moderately strong relationships were indicated for phase 6 for Z500 but for no other phase when considering SAT. These correlation coefficients suggest that for May, physical agreement between snow depth changes and midtropospheric

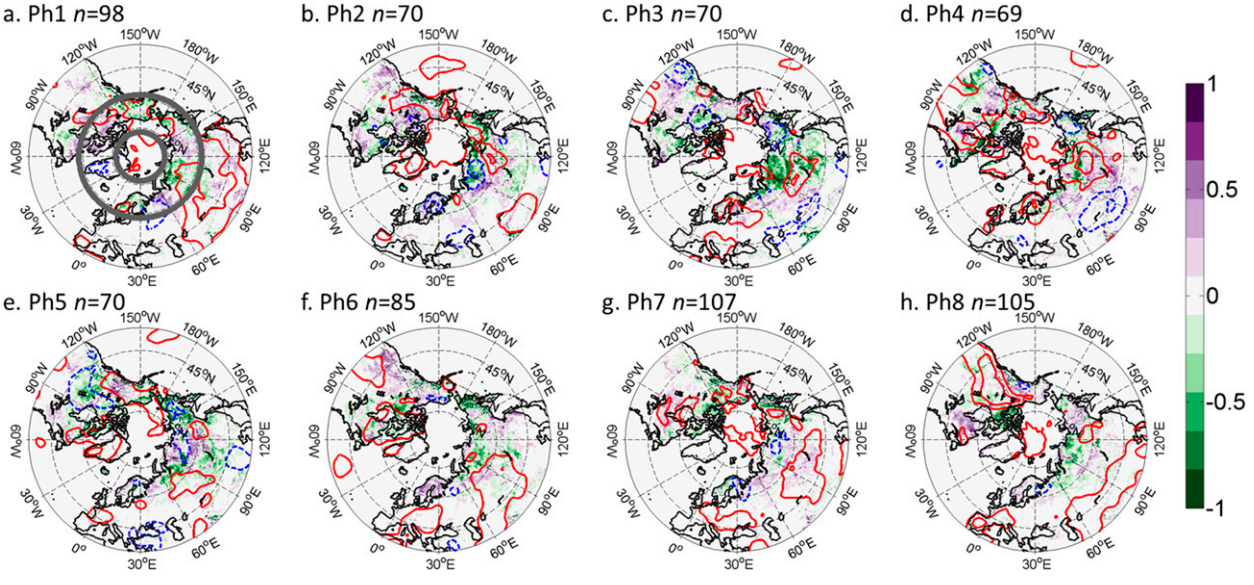

FIG. 7. (a)–(h) As in Fig. 3, but for May 1980–2013 snow depth change (shaded) and surface air temperature (blue and red contoured) anomalies. North American sector indicated in (a) by the gray bounded region includes all longitudes from 60° to 75°N.

TABLE 3. As in Table 1, but for May 1980–2013. The Northern Hemisphere sector includes all longitudes in the latitude band from 60° to 75°N.

May	Phase 1	Phase 2	Phase 3	Phase 4	Phase 5	Phase 6	Phase 7	Phase 8
Northern Hemisphere Z500	**−0.49**	−0.34	−0.27	−0.14	−0.08	−0.41	−0.26	−0.30
Northern Hemisphere SAT	**−0.38**	0.05	0.15	0.07	0.08	−0.11	0.08	0.17

circulation and surface air temperature were less than March but similar to April. Finally, similar to March and April, when correlation coefficients for May were calculated for all of North America and Eurasia, correlations were found to be smaller (closer to zero) for both SAT and Z500 (not shown).

4. Discussion and conclusions

Here, for the first time, variability in springtime Northern Hemisphere snow depth by phase of the MJO was explored. Statistically significant regions of daily snow depth change (ΔSD) anomalies were found in March, April, and May in both North America and Eurasia. The magnitude of observed anomalies in ΔSD in some regions was found to exceed 100% of the monthly mean change, indicating intraseasonal variability of spring-season daily snow depth change was physically significant. From March to May, regions of greatest ΔSD anomalies progressed poleward, following the seasonal shift in the ephemeral snow zone. Seven days after active phase 5 and 7 occurrences in March, synoptic-scale wavy anomalies in Z500 and SAT were found extending across the Northern Hemisphere, generally collocated with ΔSD anomalies of the opposite sign. Correlation coefficients over sectors in both Eurasia and North America approached −0.6, indicating a moderate to strong physical relationship between ΔSD and both midtroposphere circulation and surface air temperature. In April, a similar statistical relationship was seen between Z500 and ΔSD 7 days after active phase 1 and 5 occurrences over Eurasia, but only a weak relationship was found between ΔSD and SAT. In May, moderately strong statistical relationships between ΔSD and Z500 and ΔSD and SAT were found 7 days after active phase 1 days. This decline in correlation coefficients between March and May suggests that the best intraseasonal agreement between the atmosphere and ΔSD occurs in March, with somewhat lesser agreement in April and May.

As introduced in the results section, we propose the following physical mechanism to explain intraseasonal variability of ΔSD. This mechanism is based on the statistical relationships found between spring-season ΔSD and both Z500 and SAT and on the known intraseasonal variability of extratropical circulation with active MJO. The components of this mechanism include poleward-propagating Rossby waves that, in response to tropical MJO convection, interact with background flow over the Northern Hemisphere, leading to anomalous troughing and ridging, including at 500 hPa. These anomalous circulation centers then directly impact daily snow depth change via synoptic-scale precipitation processes, with ascent (and precipitation) favored in troughing and descent (and no precipitation) favored in ridging. Anomalous troughing and ridging also indirectly impact snow depth via anomalies in surface temperature, with colder temperatures associated with anomalous troughing and warmer temperatures associated with anomalous ridging. However, each phase was found to behave differently, and correlation coefficients never exceeded −0.6, both likely products of the fact that the MJO is not the only driver of spring-season changes in snow depth. Future work should focus on the covariability of ΔSD with both the MJO and other leading atmospheric modes of variability, including the Arctic Oscillation, North Atlantic Oscillation, and Pacific–North America pattern.

Acknowledgments. This work was partially sponsored by National Science Foundation Award PLR-1203843. We thank the anonymous reviewers for their helpful comments and feedback.

REFERENCES

Adames, Á. F., and J. M. Wallace, 2014: Three-dimensional structure and evolution of the MJO and its relation to the mean flow. *J. Atmos. Sci.,* **71,** 2007–2026, doi:10.1175/JAS-D-13-0254.1.

Bao, M., and D. L. Hartmann, 2014: The response to MJO-like forcing in a nonlinear shallow-water model. *Geophys. Res. Lett.,* **41,** 1322–1328, doi:10.1002/2013GL057683.

Barlow, M., 2012: Africa and west Asia. *Intraseasonal Variability in the Atmosphere-Ocean Climate System,* 2nd ed. W. K. M. Lau and D. E. Waliser, Eds., Springer, 477–495.

Barrett, B. S., and V. Gensini, 2013: Modulation of daily United States April–May tornado day likelihood by phase of the Madden–Julian oscillation. *Geophys. Res. Lett.,* **40,** 2790–2795, doi:10.1002/grl.50522.

Baxter, S., S. Weaver, J. Gottschalck, and Y. Xue, 2014: Pentad evolution of wintertime impacts of the Madden–Julian oscillation over the contiguous United States. *J. Climate,* **27,** 7356–7367, doi:10.1175/JCLI-D-14-00105.1.

Becker, E. J., E. H. Berbery, and R. W. Higgins, 2011: Modulation of cold-season U.S. daily precipitation by the Madden–Julian oscillation. *J. Climate,* **24,** 5157–5166, doi:10.1175/2011JCLI4018.1.

Bladé, I., and D. L. Hartmann, 1995: The linear and nonlinear extratropical response to tropical intraseasonal heating. *J. Atmos. Sci.,* **52,** 4448–4471, doi:10.1175/1520-0469(1995)052<4448:TLANER>2.0.CO;2.

Bond, N. A., and G. A. Vecchi, 2003: The influence of the Madden–Julian oscillation on precipitation in Oregon and Washington. *Wea. Forecasting,* **18,** 600–613, doi:10.1175/1520-0434(2003)018<0600:TIOTMO>2.0.CO;2.

Brown, R. D., and P. W. Mote, 2009: The response of Northern Hemisphere snow cover to a changing climate. *J. Climate,* **22,** 2124–2145, doi:10.1175/2008JCLI2665.1.

Cassou, C., 2008: Intraseasonal interaction between the Madden–Julian oscillation and the North Atlantic Oscillation. *Nature,* **455,** 523–527, doi:10.1038/nature07286.

Cohen, J., and D. Rind, 1991: The effect of snow cover on the climate. *J. Climate,* **4,** 689–706, doi:10.1175/1520-0442(1991)004<0689:TEOSCO>2.0.CO;2.

Derksen, C., and E. LeDrew, 2000: Variability and change in terrestrial snow cover: Data acquisition and links to the atmosphere. *Prog. Phys. Geogr.,* **24,** 469–498, doi:10.1177/030913330002400401.

——, and R. Brown, 2012: Spring snow cover extent reductions in the 2008–2012 period exceeding climate model predictions. *Geophys. Res. Lett.,* **39,** L19504, doi:10.1029/2012GL053387.

——, ——, L. Mudryk, and K. Luojus, 2014: Terrestrial snow cover. [Available online at http://www.arctic.noaa.gov/reportcard/snow_cover.html.]

Déry, S. J., and R. D. Brown, 2007: Recent Northern Hemisphere snow cover extent trends and implications for the snow-albedo feedback. *Geophys. Res. Lett.,* **34,** L22504, doi:10.1029/2007GL031474.

Flatau, M., and Y.-J. Kim, 2013: Interaction between the MJO and polar circulations. *J. Climate,* **26,** 3562–3574, doi:10.1175/JCLI-D-11-00508.1.

Francis, J. A., and S. J. Vavrus, 2015: Evidence for a wavier jet stream in response to rapid Arctic warming. *Environ. Res. Lett.,* **10,** 014005, doi:10.1088/1748-9326/10/1/014005.

Garfinkel, C. I., J. J. Benedict, and E. D. Maloney, 2014: Impact of the MJO on the boreal winter extratropical circulation. *Geophys. Res. Lett.,* **41,** 6055–6062, doi:10.1002/2014GL061094.

Ge, Y., and G. Gong, 2008: Observed inconsistencies between snow extent and snow depth variability at regional/continental scales. *J. Climate,* **21,** 1066–1082, doi:10.1175/2007JCLI1829.1.

Goss, M., and S. B. Feldstein, 2015: The impact of the initial flow on the extratropical response to Madden–Julian oscillation convective heating. *Mon. Wea. Rev.,* **143,** 1104–1121, doi:10.1175/MWR-D-14-00141.1.

Guan, B., D. E. Waliser, N. P. Molotch, E. J. Fetzer, and P. J. Neiman, 2012: Does the Madden–Julian oscillation influence wintertime atmospheric rivers and snowpack in the Sierra Nevada? *Mon. Wea. Rev.,* **140,** 325–342, doi:10.1175/MWR-D-11-00087.1.

Gutzler, D. S., 2000: Covariability of spring snowpack and summer rainfall across the southwest United States. *J. Climate,* **13,** 4018–4027, doi:10.1175/1520-0442(2000)013<4018:COSSAS>2.0.CO;2.

——, and J. W. Preston, 1997: Evidence for a relationship between spring snow cover in North America and summer rainfall in New Mexico. *Geophys. Res. Lett.,* **24,** 2207–2210, doi:10.1029/97GL02099.

Hall, A., X. Qu, and J. D. Neelin, 2008: Improving predictions of summer climate change in the United States. *Geophys. Res. Lett.,* **35,** L01702, doi:10.1029/2007GL032012.

He, J., H. Lin, and Z. Wu, 2011: Another look at influences of the Madden-Julian oscillation on the wintertime East Asian weather. *J. Geophys. Res.,* **116,** D03109, doi:10.1029/2010JD014787.

Henderson, G. R., B. S. Barrett, and D. M. Lafleur, 2014: Arctic sea ice and the Madden–Julian oscillation (MJO). *Climate Dyn.,* **43,** 2185–2196, doi:10.1007/s00382-013-2043-y.

Hendon, H. H., and M. L. Salby, 1994: The life cycle of the Madden–Julian oscillation. *J. Atmos. Sci.,* **51,** 2225–2237, doi:10.1175/1520-0469(1994)051<2225:TLCOTM>2.0.CO;2.

Higgins, R. W., and K. C. Mo, 1997: Persistent North Pacific circulation anomalies and the tropical intraseasonal oscillation. *J. Climate,* **10,** 223–244, doi:10.1175/1520-0442(1997)010<0223:PNPCAA>2.0.CO;2.

Hoskins, B. J., and D. J. Karoly, 1981: The steady linear response of a spherical atmosphere to thermal and orographic forcing. *J. Atmos. Sci.,* **38,** 1179–1196, doi:10.1175/1520-0469(1981)038<1179:TSLROA>2.0.CO;2.

Jackson, S. I., T. D. Prowse, and B. R. Bonsal, 2014: Linkages between snow ablation and atmospheric boundary-layer conditions in a semi-arid basin of western Canada. *J. Hydrol.,* **517,** 949–962, doi:10.1016/j.jhydrol.2014.06.010.

Jeong, J. H., B. M. Kim, C. H. Ho, and Y. H. Noh, 2008: Systematic variation in wintertime precipitation in East Asia by MJO-induced extratropical vertical motion. *J. Climate,* **21,** 788–801, doi:10.1175/2007JCLI1801.1.

Jin, F., and B. J. Hoskins, 1995: The direct response to tropical heating in a baroclinic atmosphere. *J. Atmos. Sci.,* **52,** 307–319, doi:10.1175/1520-0469(1995)052<0307:TDRTTH>2.0.CO;2.

Johnson, N. C., and S. B. Feldstein, 2010: The continuum of North Pacific sea level pressure patterns: Intraseasonal, interannual, and interdecadal variability. *J. Climate,* **23,** 851–867, doi:10.1175/2009JCLI3099.1.

——, D. C. Collins, S. B. Feldstein, M. L. L'Heureux, and E. E. Riddle, 2014: Skillful wintertime North American temperature forecasts out to 4 weeks based on the state of ENSO and the MJO. *Wea. Forecasting,* **29,** 23–38, doi:10.1175/WAF-D-13-00102.1.

Jones, C., and L. M. V. Carvalho, 2014: Sensitivity to Madden–Julian oscillation variations on heavy precipitation over the contiguous United States. *Atmos. Res.,* **147–148,** 10–26, doi:10.1016/j.atmosres.2014.05.002.

——, D. E. Waliser, K. M. Lau, and W. Stern, 2004: The Madden–Julian oscillation and its impact on Northern Hemisphere weather predictability. *Mon. Wea. Rev.,* **132,** 1462–1471, doi:10.1175/1520-0493(2004)132<1462:TMOAII>2.0.CO;2.

Kanamitsu, M., W. Ebisuzaki, J. Woollen, S.-K. Yang, J. J. Hnilo, M. Fiorino, and G. L. Potter, 2002: NCEP–DOE AMIP-II Reanalysis (R-2). *Bull. Amer. Meteor. Soc.,* **83,** 1631–1643, doi:10.1175/BAMS-83-11-1631.

Kang, I.-S., and H.-M. Kim, 2010: Assessment of MJO predictability for boreal winter with various statistical and dynamical models. *J. Climate,* **23,** 2368–2378, doi:10.1175/2010JCLI3288.1.

Kiladis, G., K. H. Straub, and P. T. Haertel, 2005: Zonal and vertical structure of the Madden–Julian oscillation. *J. Atmos. Sci.,* **62,** 2790–2809, doi:10.1175/JAS3520.1.

Koster, R. D., S. P. P. Mahanama, B. Livneh, D. P. Lettenmaier, and R. H. Reichle, 2010: Skill in streamflow forecasts derived from large-scale estimates of soil moisture and snow. *Nat. Geosci.,* **3,** 613–616, doi:10.1038/ngeo944.

Lau, K. M., and T. J. Phillips, 1986: Coherent fluctuations of extratropical geopotential height and tropical convection in

intraseasonal time scales. *J. Atmos. Sci.,* **43,** 1164–1181, doi:10.1175/1520-0469(1986)043<1164:CFOFGH>2.0.CO;2.

L'Heureux, M. L., and R. W. Higgins, 2008: Boreal winter links between the Madden–Julian oscillation and the Arctic Oscillation. *J. Climate,* **21,** 3040–3050, doi:10.1175/2007JCLI1955.1.

Lin, H., 2015: Subseasonal variability of North American wintertime surface air temperature. *Climate Dyn.,* doi:10.1007/s00382-014-2363-6, in press.

——, and G. Brunet, 2009: The influence of the Madden–Julian oscillation on Canadian wintertime surface air temperature. *Mon. Wea. Rev.,* **137,** 2250–2262, doi:10.1175/2009MWR2831.1.

——, ——, and J. Derome, 2009: An observed connection between the North Atlantic Oscillation and the Madden–Julian oscillation. *J. Climate,* **22,** 4130–4149, doi:10.1175/2008JCLI2515.1.

——, ——, and R. Mo, 2010: Impact of the Madden–Julian oscillation on wintertime precipitation in Canada. *Mon. Wea. Rev.,* **138,** 3822–3839, doi:10.1175/2010MWR3363.1.

Madden, R., and P. Julian, 1971: Detection of a 40–50 day oscillation in the zonal wind in the tropical Pacific. *J. Atmos. Sci.,* **28,** 702–708, doi:10.1175/1520-0469(1971)028<0702:DOADOI>2.0.CO;2.

——, and ——, 1972: Description of global-scale circulation cells in the tropics with a 40–50 day period. *J. Atmos. Sci.,* **29,** 1109–1123, doi:10.1175/1520-0469(1972)029<1109:DOGSCC>2.0.CO;2.

——, and ——, 1994: Observations of the 40–50-day tropical oscillation—A review. *Mon. Wea. Rev.,* **122,** 814–837, doi:10.1175/1520-0493(1994)122<0814:OOTDTO>2.0.CO;2.

Mahanama, S., B. Livneh, R. Koster, D. Lettenmaier, and R. Reichle, 2012: Soil moisture, snow, and seasonal streamflow forecasts in the United States. *J. Hydrometeor.,* **13,** 189–203, doi:10.1175/JHM-D-11-046.1.

Mankin, J. S., and N. S. Diffenbaugh, 2015: Influence of temperature and precipitation variability on near-term snow trends. *Climate Dyn.,* **45,** 1099–1116, doi:10.1007/s00382-014-2357-4.

Matsumura, S., X. Zhang, and K. Yamazaki, 2014: Summer Arctic atmospheric circulation response to spring Eurasian snow cover and its possible linkage to accelerated sea ice decrease. *J. Climate,* **27,** 6551–6558, doi:10.1175/JCLI-D-13-00549.1.

Matthews, A. J., B. J. Hoskins, and M. Masutani, 2004: The global response to tropical heating in the Madden–Julian oscillation during the northern winter. *Quart. J. Roy. Meteor. Soc.,* **130,** 1991–2011, doi:10.1256/qj.02.123.

Monteiro, J. M., Á. F. Adames, J. M. Wallace, and J. S. Sukhatme, 2014: Interpreting the upper level structure of the Madden-Julian oscillation. *Geophys. Res. Lett.,* **41,** 9158–9165, doi:10.1002/2014GL062518.

Mori, M., and M. Watanabe, 2008: The growth and triggering mechanisms of the PNA: A MJO-PNA coherence. *J. Meteor. Soc. Japan,* **86,** 213–236, doi:10.2151/jmsj.86.213.

Neena, J. M., J. Y. Lee, D. Waliser, B. Wang, and X. Jiang, 2014: Predictability of the Madden–Julian oscillation in the Intraseasonal Variability Hindcast Experiment (ISVHE). *J. Climate,* **27,** 4531–4543, doi:10.1175/JCLI-D-13-00624.1.

Oliver, E. J. C, 2015: Multidecadal variations in the modulation of Alaska wintertime air temperature by the Madden–Julian oscillation. *Theor. Appl. Climatol.,* **121,** 1–11, doi:10.1007/s00704-014-1215-y.

Quiring, S. M., and D. B. Kluver, 2009: Relationship between winter/spring snowfall and summer precipitation in the northern Great Plains of North America. *J. Hydrometeor.,* **10,** 1203–1217, doi:10.1175/2009JHM1089.1.

Reichle, R. H., R. D. Koster, G. J. M. De Lannoy, B. A. Forman, Q. Liu, S. P. P. Mahanama, and A. Touré, 2011: Assessment and enhancement of MERRA land surface hydrology estimates. *J. Climate,* **24,** 6322–6338, doi:10.1175/JCLI-D-10-05033.1.

Riddle, E. E., M. B. Stoner, N. C. Johnson, M. L. L'Heureux, D. C. Collins, and S. B. Feldstein, 2013: The impact of the MJO on clusters of wintertime circulation anomalies over the North American region. *Climate Dyn.,* **40,** 1749–1766, doi:10.1007/s00382-012-1493-y.

Rienecker, M. M., and Coauthors, 2011: MERRA: NASA's Modern-Era Retrospective Analysis for Research and Applications. *J. Climate,* **24,** 3624–3648, doi:10.1175/JCLI-D-11-00015.1.

Robinson, D. A., K. F. Dewey, and R. R. Heim, 1993: Global snow cover monitoring: An update. *Bull. Amer. Meteor. Soc.,* **74,** 1689–1696, doi:10.1175/1520-0477(1993)074<1689:GSCMAU>2.0.CO;2.

Rodney, M., H. Lin, and J. Derome, 2013: Subseasonal prediction of wintertime North American surface air temperature during strong MJO events. *Mon. Wea. Rev.,* **141,** 2897–2909, doi:10.1175/MWR-D-12-00221.1.

Roundy, P. E., 2012: Tropical extratropical interactions. *Intraseasonal Variability in the Atmosphere-Ocean Climate System,* 2nd ed. W. K. M. Lau and D. E. Waliser, Eds., Springer, 497–512.

——, K. MacRitchie, J. Asuma, and T. Melino, 2010: Modulation of the global atmospheric circulation by combined activity in the Madden–Julian oscillation and the El Niño–Southern Oscillation during boreal winter. *J. Climate,* **23,** 4045–4059, doi:10.1175/2010JCLI3446.1.

Rydzik, M., and A. R. Desai, 2014: Relationship between snow extent and midlatitude disturbance centers. *J. Climate,* **27,** 2971–2982, doi:10.1175/JCLI-D-12-00841.1.

Sardeshmukh, P. D., and B. J. Hoskins, 1988: The generation of global rotational flow by steady idealized tropical divergence. *J. Atmos. Sci.,* **45,** 1228–1251, doi:10.1175/1520-0469(1988)045<1228:TGOGRF>2.0.CO;2.

Seo, K. H., and S. W. Son, 2012: The global atmospheric circulation response to tropical diabatic heating associated with the Madden–Julian oscillation during northern winter. *J. Atmos. Sci.,* **69,** 79–96, doi:10.1175/2011JAS3686.1.

Su, H., R. E. Dickinson, K. L. Findell, and B. R. Lintner, 2013: How are spring snow conditions in central Canada related to early warm-season precipitation? *J. Hydrometeor.,* **14,** 787–807, doi:10.1175/JHM-D-12-029.1.

Trenberth, K. E., J. T. Fasullo, and J. Mackaro, 2011: Atmospheric moisture transports from ocean to land and global energy flows in reanalyses. *J. Climate,* **24,** 4907–4924, doi:10.1175/2011JCLI4171.1.

Virts, K. S., J. M. Wallace, M. L. Hutchins, and R. H. Holzworth, 2013: Diurnal lightning variability over the Maritime Continent: Impact of low-level winds, cloudiness, and the MJO. *J. Atmos. Sci.,* **70,** 3128–3146, doi:10.1175/JAS-D-13-021.1.

Vitart, F., and F. Molteni, 2010: Simulation of the Madden–Julian oscillation and its teleconnections in the ECMWF forecast system. *Quart. J. Roy. Meteor. Soc.,* **136,** 842–855, doi:10.1002/qj.623.

Wallace, J. M., and D. S. Gutzler, 1981: Teleconnections in the geopotential height field during the Northern Hemisphere winter. *Mon. Wea. Rev.,* **109,** 784–812, doi:10.1175/1520-0493(1981)109<0784:TITGHF>2.0.CO;2.

Wang, T., S. Peng, C. Ottlé, and P. Ciais, 2015: Spring snow cover deficit controlled by intraseasonal variability of the surface energy fluxes. *Environ. Res. Lett.,* **10,** 024018, doi:10.1088/1748-9326/10/2/024018.

Weickmann, K., and E. Berry, 2009: The tropical Madden–Julian oscillation and the global wind oscillation. *Mon. Wea. Rev.,* **137,** 1601–1614, doi:10.1175/2008MWR2686.1.

Wheeler, M., and H. H. Hendon, 2004: An all-season real-time multivariate MJO index: Development of an index for monitoring and prediction. *Mon. Wea. Rev.,* **132,** 1917–1932, doi:10.1175/1520-0493(2004)132<1917:AARMMI>2.0.CO;2.

Yao, W., H. Lin, and J. Derome, 2011: Submonthly forecasting of winter surface air temperature in North America based on organized tropical convection. *Atmos.–Ocean,* **49,** 51–60, doi:10.1080/07055900.2011.556882.

Yoo, C., S. Feldstein, and S. Lee, 2011: The impact of the Madden-Julian oscillation trend on the Arctic amplification of surface air temperature during the 1979–2008 boreal winter. *Geophys. Res. Lett.,* **38,** L24804, doi:10.1029/2011GL049881.

——, S. Lee, and S. B. Feldstein, 2012: Mechanisms of Arctic surface air temperature change in response to the Madden–Julian oscillation. *J. Climate,* **25,** 5777–5790, doi:10.1175/JCLI-D-11-00566.1.

——, S. B. Feldstein, and S. Lee, 2014: The prominence of a tropical convective signal in the wintertime Arctic temperature. *Atmos. Sci. Lett.,* **15,** 7–12, doi:10.1002/asl2.455.

Zakharova, E. A., A. V. Kouraev, S. Biancamaria, M. V. Kolmakova, N. M. Mognard, V. A. Zemtsov, S. N. Kirpotin, and B. Decharme, 2011: Snow cover and spring flood flow in the northern part of western Siberia (the Poluy, Nadym, Pur, and Taz Rivers). *J. Hydrometeor.,* **12,** 1498–1511, doi:10.1175/JHM-D-11-017.1.

Zhang, C., 2005: Madden–Julian oscillation. *Rev. Geophys.,* **43,** RG2003, doi:10.1029/2004RG000158.

——, 2013: Madden–Julian oscillation: Bridging weather and climate. *Bull. Amer. Meteor. Soc.,* **94,** 1849–1870, doi:10.1175/BAMS-D-12-00026.1.

Zhou, S., and A. J. Miller, 2005: The interaction of the Madden–Julian oscillation and the Arctic Oscillation. *J. Climate,* **18,** 143–159, doi:10.1175/JCLI3251.1.

——, M. L'Heureux, S. Weaver, and A. Kumar, 2012: A composite study of the MJO influence on the surface air temperature and precipitation over the continental United States. *Climate Dyn.,* **38,** 1459–1471, doi:10.1007/s00382-011-1001-9.

Zhu, C. M., D. P. Lettenmaier, and T. Cavazos, 2005: Role of antecedent land surface conditions on North American monsoon rainfall variability. *J. Climate,* **18,** 3104–3121, doi:10.1175/JCLI3387.1.

——, T. Cavazos, and D. P. Lettenmaier, 2007: Role of antecedent land surface conditions in warm season precipitation over northwestern Mexico. *J. Climate,* **20,** 1774–1791, doi:10.1175/JCLI4085.1.

Zhu, H., M. C. Wheeler, A. H. Sobel, and D. Hudson, 2014: Seamless precipitation prediction skill in the tropics and extratropics from a global model. *Mon. Wea. Rev.,* **142,** 1556–1569, doi:10.1175/MWR-D-13-00222.1.